








RESEARCH ARTICLE

Ion mobility mass spectrometry of saponin ions

Corentin Decroo^{1,2,3}  | Emmanuel Colson^{1,3} | Vincent Lemaur²  | Guillaume Caulier³  | Julien De Winter¹  | Gustavo Cabrera-Barjas⁴ | Jérôme Cornil²  | Patrick Flammang³  | Pascal Gerbaux¹ 

¹Organic Synthesis and Mass Spectrometry Lab, Interdisciplinary Center for Mass Spectrometry, Research Institute for Biosciences, University of Mons – UMONS, 23 Place du Parc, B-7000 Mons, Belgium

²Laboratory for Chemistry of Novel Materials, Center of Innovation and Research in Materials and Polymers, Research Institute for Science and Engineering of Materials, University of Mons – UMONS, 23 Place du Parc, 7000 Mons, Belgium

³Biology of Marine Organisms and Biomimetics Unit, Research Institute for Biosciences, University of Mons – UMONS, 23 Place du Parc, B-7000 Mons, Belgium

⁴Unit for Technology Development (UDT), University of Concepción, Av. Cordillera 2634, Parque Industrial Coronel, P.O. Box 4051 mail 3 Coronel, Región del Bío Bío, Chile

Correspondence

P. Gerbaux, Organic Synthesis and Mass Spectrometry Lab, Interdisciplinary Center for Mass Spectrometry, Research Institute for Biosciences, University of Mons – UMONS, 23 Place du Parc, B-7000 Mons, Belgium.
Email: pascal.gerbaux@umons.ac.be

Rationale: Saponins are natural compounds presenting a high structural diversity whose structural characterization remains extremely challenging. Ideally, saponin structures are best established using nuclear magnetic resonance experiments conducted on isolated molecules. However, saponins are also increasingly characterized using tandem mass spectrometry (MS/MS) coupled with liquid chromatography, even if collision-induced dissociation (CID) experiments are often quite limited in accurately determining the saponin structure.

Methods: We consider here ion mobility mass spectrometry (IMMS) as an orthogonal tool for the structural characterization of saponin isomers by comparing the experimental collisional cross sections (CCSs) of saponin ions with theoretical CCSs for candidate ion structures. Indeed, state-of-the-art theoretical calculations perfectly complement the experimental results, allowing the ion structures to be deciphered at the molecular level.

Results: We demonstrate that ion mobility can contribute to the structural characterization of saponins because different saponin ions present significantly distinct CCSs. Depending on the nature of the cation (in the positive ion mode), the differences in CCSs can also be exacerbated, optimizing the gas-phase separation. When associated with molecular dynamics simulations, the CCS data can be used to describe the interactions between the cations, i.e. H⁺, Na⁺ and K⁺, and the saponin molecules at a molecular level.

Conclusions: Our work contributes to resolve the relationship between the primary and secondary structures of saponin ions. However, it is obvious that the structural diversity and complexity of the saponins cannot be definitively unraveled by measuring a single numerical value, here the CCS. Consequently, the structural characterization of unknown saponins will be difficult to achieve based on IMMS alone. Nevertheless, we demonstrated that monodesmosidic and bidesmosidic saponins can be distinguished via IMMS.

1 | INTRODUCTION

Saponins are natural glycosides formally arising from the condensation of a saccharide chain – the glycone – onto a lipophilic triterpene – the aglycone. The polar part is constituted by a linear or ramified oligosaccharide in which the nature and number of the

monosaccharide residues can differ. The apolar part is constructed around a sterol or a triterpenoid base.^{1,2} Those biomolecules are present in numerous plants^{3–6} but also in different classes of echinoderms, in particular in sea stars^{7–11} and sea cucumbers.^{12–17} Thanks to their amphiphilic property and to their broad structural diversity, saponin molecules are considered to be important candidates

in the pharmaceutical and food industries as well as in agronomy.^{5,9,18-23} Nevertheless, as for other natural products, the principal issues to the industrial/medicinal application of saponins remain their challenging purification as well as their in-depth structural characterization. This is particularly true for this family of molecules since extracts are usually made up of complex mixtures of structurally related saponins. A complete saponin characterization also represents a prerequisite to assess their structure/activity relationships. For many years, saponin structures have been established based on a time-consuming procedure combining individual saponin isolation and nuclear magnetic resonance (NMR) measurements.^{3,7,9,20,24-28} Nowadays, mass spectrometry methods are increasingly involved for their structural identification based on accurate mass measurements (high-resolution mass spectrometry – HRMS) and collision-induced dissociation (CID) experiments.^{4,12,14,17,29-31} Mass spectrometry data are almost always interpreted based on NMR results and it is important to remind here that MS alone is unable to distinguish stereoisomers. Note also that isomeric saponins even present sometimes similar dissociation patterns upon CID.^{8,29,32-34} Recently, the capabilities of Ion Mobility Mass Spectrometry (IMMS) to define the primary as well as secondary structures of (bio) molecules have been abundantly tested and promising results have already been reported in the literature on proteins,³⁵ synthetic polymers³⁶ and small molecules.³⁷⁻³⁹ Moreover, the use of IMMS for the study of secondary metabolites, such as flavonoids,^{40,41} isomeric flavanols,⁴² stevioside and rebaudioside glycosides⁴³ has started to be documented. In a recent publication, we described a global MS-based methodology for saponin extract analysis that associates matrix-assisted laser desorption/ionization time-of-flight (MALDI-TOF), HRMS, liquid chromatography (LC)/MS, CID and IMMS. We took advantage of that paper to report our preliminary results dealing with the structural characterization of saponins by IMMS coupled to computational chemistry.³¹ The principal outcome of this initial study was that ion mobility data are not currently sufficient to discriminate different isomers presenting similar structures, which is often the case when considering the extract from a natural source. The ionization of the saponin molecules within the ion source of the mass spectrometer warrants the MS analysis and detection of the saponin ions but induces the folding of the saponin molecule around the cation (Na^+), merging the small structure differences within a global 3D ion structure.³¹

Instead of considering the use of ion mobility to distinguish closely related saponins, we suspect that IMMS can be more efficient in differentiating topological isomers of saponins. Saponin congeners can be roughly classified according to the number of polysaccharide chains appended to the aglycone moiety. Monodesmosidic saponins are characterized by the condensation of a single oligosaccharide onto the aglycone, whereas polydesmosidic structures appear when several oligosaccharide chains are grafted onto the aglycone. Beside these two families, macrocyclic topologies are also known and correspond to molecules with single oligosaccharide chains attached at two sites of the aglycone. These topologies require extensive purification and subsequent NMR experiments to be identified.⁴⁴⁻⁴⁶ In the context of our development of MS-based methods for saponin characterization, we here consider IMMS, in association with computational chemistry, for the

distinction between saponins presenting different topologies. For the present study, we select the sea cucumber *Holothuria forskali*, the common soy *Glycine max*, and the quinoa *Chenopodium quinoa* as saponin sources, since their saponin extracts are known to be constituted by monodesmosidic saponins,^{16,25} a mixture of mono- and bidesmosidic molecules,^{29,47,48} and bidesmosidic structures only,^{33,49} respectively.

2 | EXPERIMENTAL

2.1 | Chemicals, animal and plant sampling, and saponin extractions

For saponin extractions and mass spectrometry analyses, technical grade methanol, hexane, dichloromethane, chloroform and isobutanol, as well as HPLC grade water, acetonitrile and methanol, were purchased from CHEM-LAB NV (Somme-Leuze, Belgium). *N,N*-Dimethylaniline (DMA) and 2,5-dihydroxybenzoic acid (DHB) were provided by Sigma-Aldrich (Diegem, Belgium).

Individuals of *Holothuria forskali* (Delle Chiaje, 1823) were obtained from the Observatoire Océanologique of Banyuls-sur-Mer (France) during autumn 2016. They were transported to the University of Mons, where they were kept in a marine aquarium with closed circulation (20°C, pH 7.6, 33 psu). One holothuroid was dissected and its body wall was frozen (–80°C) and lyophilized (Christ alpha 1–2 freeze-dryer). The dry tissue was reduced to powder and conserved away from light. Animals used in our experiments were maintained and treated in compliance with the guidelines specified by the Belgian Ministry of Trade and Agriculture.

Soy seeds were bought from an Asian food store. The dry seeds were powdered with an IKA crusher and preserved away from light.

For the quinoa source, integuments of mature achenes were obtained from pooled samples from the Quinoa Breeding Program from INIA (Instituto Nacional de Investigación Agraria - Chile). To separate kernels from the outer husk, seeds were subjected to physical shearing to obtain quinoa grains. The remaining husks have a particle size lower than 1 mm in diameter.

The different powders undergo an extraction method adapted from Van Dyck et al.¹⁶ The weighed powder is stirred in methanol for 24 h at room temperature followed by filtration. The extracts are diluted to 70% methanol with milliQ water. These methanolic extracts are partitioned (v/v) successively against n-hexane, dichloromethane and chloroform. Finally, the hydromethanolic solution is evaporated at low pressure in a double boiler at 46°C using a rotary evaporator. The dry extract is diluted in water to undergo a last partitioning against isobutanol (v/v). The butanolic phase is washed twice with water to remove salts and impurities. The organic solution contains the saponins. However, in the case of the soy sample, an additional solid-phase extraction is required because of the presence of isoflavones after the liquid–liquid extractions. The method consists of using various concentrations of acetonitrile in water on a 500 mg C18 cartridge. After deposition of the sample on the column, isoflavones and the saponins are eluted successively with 20% and 50% of acetonitrile, respectively, to produce a relatively pure mixture

of soyasaponins. The purification yield is 4%wt, implying that we can purify 4 mg of soyasaponin mixture from 100 mg of the semi-purified extract.

2.2 | Mass spectrometry analyses

Mass spectrometry analyses consist of two steps. First, the saponin pure extract is analyzed with a Waters Q-TOF Premier mass spectrometer in the positive ion mode. The MALDI source is constituted of a Nd-YAG laser, operating at 355 nm, with a maximum pulse energy of 104.1 μJ delivered in 2.2 ns to the sample at 200 Hz repeating rate. All samples are prepared using as the matrix a mixture of 25 mg of DHB in 250 μL water/acetonitrile (v/v) with 6 μL of DMA. The dried-droplet method is selected to prepare the sample/matrix co-crystal on the target plate. In this method, the saponin extract is not premixed with the matrix. A sample droplet (1 μL) is applied on top of a fast-evaporated matrix-only bed. For the recording of the single-stage MALDI-MS spectra, the quadrupole (rf-only mode) is set to pass ions between m/z 250 and 2000 and all ions are transmitted into the pusher region of the TOF analyzer where they are mass-analyzed with an 1 s integration time.


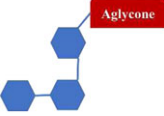

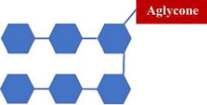



The second step consists of an on-line LC/(IM) MS analysis with a Waters Alliance 2695 liquid chromatography device coupled to a Waters Synapt G2-Si mass spectrometer. The HPLC part consists of a vacuum degasser, a quaternary pump and an autosampler. Sample volumes of 1 μL are injected. Chromatographic separation is performed on a non-polar column (Eclipse plus C18; 4.6 \times 100 mm; 3.5 μm ; Agilent) at 40°C. The mobile phase is set with a constant flow rate (1 mL/min) and the following elution gradient: (1) 85% of eluent A (water, 0.1% formic acid) and 15% of eluent B (acetonitrile) to 60% of eluent A and 40% of eluent B during the first 6 min; (2) 60% of eluent A and 40% eluent B for the next 10 min; (3) move towards 5% eluent A and 95% eluent B for 5 min; and (4) back to 85% eluent A and 15% eluent B at the end of the 20-min chromatographic run. For the mass spectrometer parameters, the ESI conditions are: positive ion mode; capillary voltage 2.5 kV; cone voltage 40 V; source offset 80 V; source temperature 100°C; desolvation temperature 300°C. Dry nitrogen is used as the ESI gas at a flow rate of 500 L/h for the desolvation gas. The single-stage LC/MS spectra are recorded by using the TOF analyzer (m/z 250 and 2000). For the LC/MS/MS experiments, the ions of interest are mass-selected by the quadrupole. The selected ions are then submitted to collision against argon in the trap cell of the Tri-Wave device and the laboratory frame kinetic energy (Elab) is selected to afford intense enough product ion signals. The product ions are finally mass measured with the TOF analyzer. After chromatographic optimizations, the ion mobility experiments are performed using the TWIMS cell constituting the so-called Tri-Wave setup, composed of three successive T-wave elements named the Trap cell, the IMS cell, and the Transfer cell, in which the wave speed and amplitude are user-tunable. The trap and transfer cells are filled with argon whereas the IMS cell is filled with nitrogen. A small rf-only cell filled with helium is fitted between the trap and the IMS cell. This mass spectrometer is used for the recording of the ESI full scan mass spectrum, for the collision-induced dissociation (CID) as well as for the ion mobility experiments. Ion mobility parameters are tuned to have

the highest separation between different ion structures. The IMS cell conditions are gas flow 110 mL/min; wave velocity 400 m/s; wave height 40 V. TWIMS data are analyzed using the Waters MassLynx SCN 901 software. Arrival time distributions (ATDs) are recorded by selecting the most abundant isotope for each ion composition to avoid unspecific selection. ATDs are converted into collisional cross-section (CCS) distributions in helium by means of a polymer calibration following a procedure detailed in the literature⁵⁰ using commercial PEG samples with average molecular weights of 600 and 1000 $\text{g}\cdot\text{mol}^{-1}$. The CCSs in Table 1 were determined at the APEX of the CCS distributions. The ion mobility resolutions (R_{CCS} in Figure 1) are calculated by using the following equation: $R_{\text{CCS}} = \text{CCS}/\Delta\text{CCS}$.

2.3 | Molecular dynamics simulations

All cationized structures ($\text{M} + \text{H}^+$, $\text{M} + \text{Na}^+$ or $\text{M} + \text{K}^+$) reported herein correspond to the lowest energy structures obtained using the following conformational search procedure. For each saponin, different starting geometries, differing by the localization of the cation (typically three complexation sites are considered, except for the protonation as discussed in the text), have been built and optimized by quenched dynamics using the Dreiding force field,⁵¹ as implemented in the Materials Studio package 6.0.⁵² All default parameters have been used except: (i) the cut-off value for the non-bonded interactions set at 500 \AA so that none of them is neglected; (ii) the conjugated gradient algorithm is selected to achieve the geometry optimizations; (iii) Gasteiger atomic charges have been used; and (iv) the distance dependence of the electrostatic interactions follows an $1/r$ law. Due to the absence of van der Waals parameters for all alkalines in the Dreiding force field, we used for all alkaline atoms the parameters extracted from the Universal Force Field (UFF).⁵³ Note that the changes in atomic charge distributions upon protonation have been set on the H^+ and its 15 neighbors according to density functional theory (DFT) calculations from the differences in the charge distribution between neutral and protonated structures. Each optimized structure for a given saponin is then used as the starting point of successive 1 ns quenched molecular dynamics (NVT, frames optimized every 0.1 ns) at increasing temperature ($T = 300 \text{ K}$, 500 K ($\times 2$), 750 K). The lowest energy conformer obtained after each quenched MD run is used as the starting point of the next simulation. Finally, the lowest energy structures are obtained by performing a final quenched MD at room temperature (NVT, frames optimized every 0.1 ns) starting from the structure obtained after the 750 K quenched MD run. After optimization, two successive molecular dynamics of 10 ns (NVT; $T = \text{room temperature}$) are performed from the most-stable ion structure obtained during the last quenched MD. The first aims to equilibrate the system and the second to generate 500 structures (frames saved every 20 fs). The average simulated cross sections are estimated by using the exact trajectory method, as implemented in the Mobcal program^{54,55} on the basis of the calculated cross sections from the 500 frames obtained for each system during the last MD run. The standard deviation of the calculated averaged collisional cross sections (CCSs) for the investigated systems is always around 6 \AA^2 ($\sim 3\%$). Proton affinities (PAs) are estimated at the DFT level of theory (B97D/6-31G**) as the energy difference between the optimized neutral and protonated molecules.

TABLE 1 MALDI-MS and LC/MS analysis of the saponin extracts [Color table can be viewed at wileyonlinelibrary.com]

Oligosaccharide type	Name	Composition	Source	Measured mass,* [M + Na] ⁺	Retention time (tR - min)	
Monodesmosidic saponins						
	Soyasaponin III	C ₄₂ H ₆₈ O ₁₄	<i>Glycine max</i>	819.4565	15.00	
	Soyasaponin IV	C ₄₁ H ₆₆ O ₁₃		789.4474	15.67	
	Soyasaponin I	C ₄₈ H ₇₈ O ₁₈		965.5086	14.02	
	Soyasaponin II	C ₄₇ H ₇₆ O ₁₇		935.4923	14.90	
	Soyasaponin V	C ₄₈ H ₇₈ O ₁₉		981.4960	13.39	
	Soyasaponin Va				10.21	
	Soyasaponin βa	C ₅₃ H ₈₂ O ₂₀		1061.5324	18.95	
	Soyasaponin βg	C ₅₄ H ₈₄ O ₂₁	<i>Holothuria forskali</i>	1091.5354	17.50	
	Holothurinoside C	C ₅₄ H ₈₆ O ₂₃		1125.5416	13.29	
	Desholothurin A	C ₅₄ H ₈₆ O ₂₄		1141.5386	12.87	
	Unknown	C ₆₀ H ₉₆ O ₂₈		1287.5986	11.99	
	Holothurinoside E				14.54	
	Holothurinoside A	C ₆₀ H ₉₆ O ₂₉		1303.5902	11.68	
	Holothurinoside N	C ₆₁ H ₉₈ O ₂₉		1317.6030	8.70	
	Holothurinoside F	C ₆₆ H ₁₀₆ O ₃₂		1433.6560	11.94	
	Unknown 1447	C ₆₇ H ₁₀₈ O ₃₂		1447.6667	12.43	
	Holothurinoside G	C ₆₆ H ₁₀₆ O ₃₃		1449.6532	11.68	
	Holothurinoside H	C ₆₇ H ₁₀₈ O ₃₃		1463.6635	12.11	
	Holothurinoside I1	C ₆₇ H ₁₀₈ O ₃₄		1479.6592	13.14	
	Bidesmosidic saponins					
		Saponin I	C ₄₇ H ₇₆ O ₁₈	<i>Chenopodium quinoa</i>	951.4984	10.80
Saponin lac		C ₄₉ H ₇₈ O ₁₉	993.5031		21.61	
Saponin B		C ₄₈ H ₇₆ O ₂₀	995.4828		9.57	
Saponin Mac		C ₄₉ H ₇₈ O ₁₈	977.5037		10.08	
	Saponin 61	C ₅₃ H ₈₆ O ₂₃		1113.5524	10.31	
	Saponin 37	C ₅₃ H ₈₄ O ₂₄		1127.5327	8.44	
	Saponin G	C ₅₄ H ₈₆ O ₂₄		1141.5469	9.98	
	Saponin O	C ₅₄ H ₈₆ O ₂₅		1157.5377	7.98	
	Soyasaponin A5	C ₅₈ H ₉₀ O ₂₆		<i>Glycine max</i>	1225.5671	11.28
	Soyasaponin A4	C ₆₄ H ₁₀₀ O ₃₁		1387.6123	12.05	

*The HRMS spectra have been recorded and are reported in Figures S1, S3 and S4 (supporting information).

HRMS measurements are performed using m/z 965.5086, 1287.5986 and 995.4828 as the lock masses for soy, sea cucumber and quinoa saponin ions, respectively (for more details, see Figures S1, S3, and S4). All saponin ions are here presented as Na⁺ adducts.

3 | RESULTS

3.1 | Saponin selection and saponin extract analyses

Monodesmosidic and bidesmosidic saponins present in the sea cucumber, *Holothuria forskali*,^{16,25} in the quinoa, *Chenopodium quinoa*, and in the common soy, *Glycine max*,²⁹ cover a wide range of

monosaccharide residue numbers, from di- to hexasaccharide glycones, making these organisms interesting saponin sources in the context of the present investigation. The saponin compositions of the soy, quinoa, and sea cucumber extracts are first assessed by the combination of MALDI-MS/MS and LC/MS/MS, as reported in our recent paper,³¹ to confirm the presence and the structure of the selected saponin ions. Note that saponins are mostly detected upon

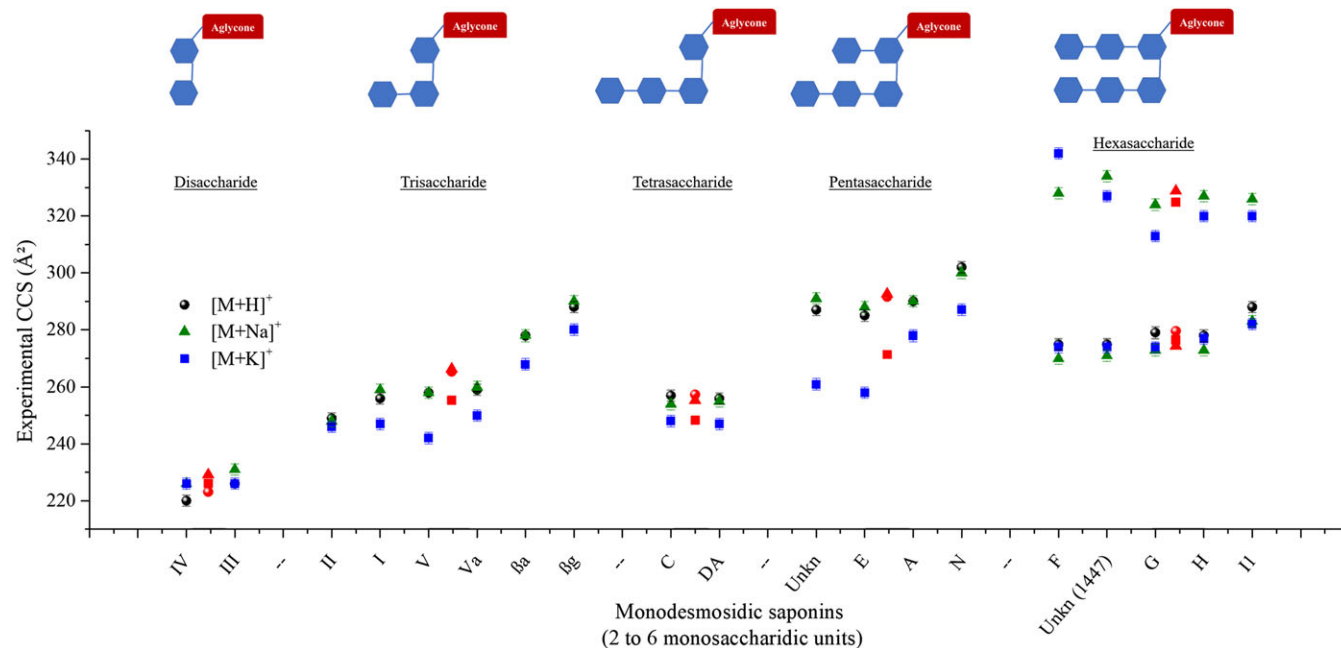


FIGURE 1 Experimental CCS for monodesmosidic saponin ions containing from 2 to 6 monosaccharide units: comparison between the $[M + H]^+$ (black), $[M + Na]^+$ (green) and $[M + K]^+$ (blue) ions. The x-axis corresponds to the different saponins investigated in the present work and labelled according to their name, see Table 1 for the correspondence. For instance, “IV” is for “Soyasaponin IV”. Standard deviation <1% is obtained for three measurements on three different days. The black circles, green triangles and blue squares respectively correspond to the $[M + H]^+$, $[M + Na]^+$ and $[M + K]^+$ ions for each saponin. The $\langle CCS_{exp} \rangle$ (in red) are calculated by averaging the CCS_{exp} values for the $[M + H]^+$ (red circles), $[M + Na]^+$ (red triangles) and $[M + K]^+$ (red squares) ions for a given number of monosaccharide residues [Color figure can be viewed at wileyonlinelibrary.com]

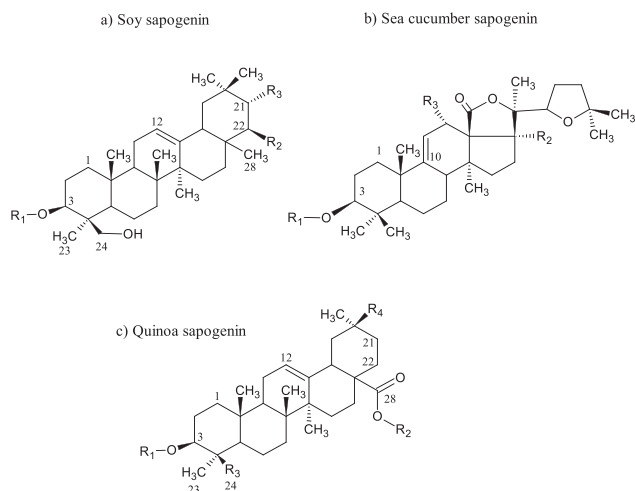
MALDI-MS and LC/MS in the positive ion mode as sodium-cationized $[M + Na]^+$ molecules, although protonated $[M + H]^+$ and potassium-cationized $[M + K]^+$ saponins are also often detected.

From the soy extract, nine saponin compositions are detected and are presented in Table 1. Their elemental compositions are confirmed by accurate mass measurements (HRMS) on the MALDI-generated saponin ions (Figure S1, supporting information). LC/MS experiments highlight the presence of ten different saponin molecules, with two isomers – two elution times – detected for the $C_{48}H_{78}O_{19}$ composition (m/z 981), see also Table 1. Based on literature data and CID experiments

(for a typical example, see Figure S2, supporting information), we confirm the presence of several known monodesmosidic saponins, namely soyasaponins I, II, III, IV, V, β_a and β_g . These different molecules are based on the same aglycone, Sapogenol B, bearing a di- or trisaccharide chain attached on its carbon 3 (C3), see Scheme 1a for a general representation and Figure S1 (supporting information) for all molecular structures.

The isomer pair detected at m/z 981 (see Table 1) is constituted by Soyasaponin V together with a new saponin. Based on CID experiments, we propose that this new molecule, named here Soyasaponin Va, contains a glycone which has the sequence R-glucuronic acid-galactose-rhamnose where R is the aglycone. The CID spectra of the two isomeric ions are significantly different (see Figure S2, supporting information) with the most significant difference corresponding to the displacement of the m/z 523 signal, for the Glc-Gal-AcG ions, toward m/z 507. This mass difference of 16 u indicates that an additional oxygen atom is present on the aglycone of the new saponin. We propose that Soyasaponin Va possesses Sapogenol A (OH group at C21, instead of H atom for Sapogenol B) as the aglycone, since Sapogenol A is the aglycone retrieved in the soy bidesmosidic saponins (see below).⁴⁸ The CID spectrum of the corresponding ions also indicates the presence of the R-Glc acid-Gal-Rha sequence (with R representing the aglycone).

The m/z 1225 and 1387 ions detected for the soy extract (Table 1) are sodium-cationized bidesmosidic saponins and the corresponding MS data (HRMS, CID) point to the presence of two known saponins,⁴⁸ namely Soyasaponin A5 (two disaccharidic chains) and A4 (di- and trisaccharidic chains), respectively (see Figure S1, supporting information). The presence of Sapogenol A as the aglycone moiety is observed in both molecules. In bidesmosidic soyasaponins, the oligosaccharidic chains are



SCHEME 1 Aglycones of (a) the *Glycine max* saponins, (b) the body wall saponins of the sea cucumber *H. forskali*, and (c) the *Chenopodium quinoa* saponins. R_{1-4} correspond to oligosaccharides or other functions. See Figures S1–S4 (supporting information) for more details

attached on the aglycone at C3 and at C22, see Scheme 1. Soyasaponins A4 and A5 are constituted by the combination of a trisaccharide at C3 plus a disaccharide at C22 – (3 + 2) connectivity – and of two disaccharide chains – (2 + 2) connectivity – respectively.

The second saponin source is the body wall of the sea cucumber (*Holothuria forskali*), a species that has been extensively investigated in our laboratory.^{16,31} Holothuroid saponins are triterpene glycosides. As presented in Scheme 1b, the structure of the aglycone moiety, a holostane-3 β -ol, is derived from the tetracyclic triterpene lanostane-3 β -ol in which the D-ring contains a γ -18(20) lactone. The oligosaccharide chain is covalently attached to the C3 of the aglycone and may include xylose, glucose, quinovose, and 3-O-methylglucose residues. We previously demonstrated the great diversity of the saponin contents in sea cucumber extracts.³¹ By submitting the body wall extract prepared for the present study to our MS-based methodology, we identified 11 saponins (see Table 1). The detected molecules are tetra-, penta- and hexasaccharide monodesmosidic saponins. As presented in Table 1, nine of those eleven molecules have already been described, but two additional molecules have still to be identified.

Finally, bidesmosidic saponins have also been extracted from quinoa. The selection of quinoa in the context of the present study is also motivated by the relative positions of the oligosaccharide chains on the aglycone (oleanic acid), with binding at C3 and C28, as opposed to the C3/C22 linkages present in the bidesmosidic soyasaponins (Scheme 1). All characterized molecules used for this study are listed in Table 1. They are identified by our MS measurements (HRMS-CID) and by comparison with structures

reported in the literature.^{33,49} All structures from quinoa present a 28-O-linked glucopyranose and a di- or trisaccharide at C3, leading to (2 + 1) and (3 + 1) connectivities, respectively.

All saponin ions – $[M + H]^+$, $[M + Na]^+$, $[M + K]^+$ – detected from the three different sources are then subjected to ion mobility measurements to determine their collisional cross sections – CCS_{exp} – while candidate structures are generated by molecular dynamics (MD) simulations. The optimized structures are injected into the Mobcal software^{54,55} to determine the CCS_{th} to be compared with the CCS_{exp} .

3.2 | Collisional cross sections of monodesmosidic saponin ions

Figure 1 gathers the experimental collisional cross sections of all **monodesmosidic** saponin ions detected from soy (2- and 3-sugar saponins) and sea cucumber (4- to 6-sugar saponins) extracts. The CCS_{exp} are grouped as a function of the increasing number of monosaccharide residues. Another parameter that will be structure-determining is the difference between the sapogenin of the di- and trisaccharides (Scheme 1a) and the tetra- to hexasaccharidic saponins (Scheme 1b). We may already anticipate that the lactone oxygen atoms of the sea cucumber saponins will participate in the charge stabilization. Unfortunately, 4-sugar soyasaponins are not detected and thus not available for comparison.

In Figure 1, we schematically represent the molecular structures of the saponin molecules. Special attention is paid to the distinction between the different cationizing agents, i.e. H^+ , Na^+ and K^+ , since these

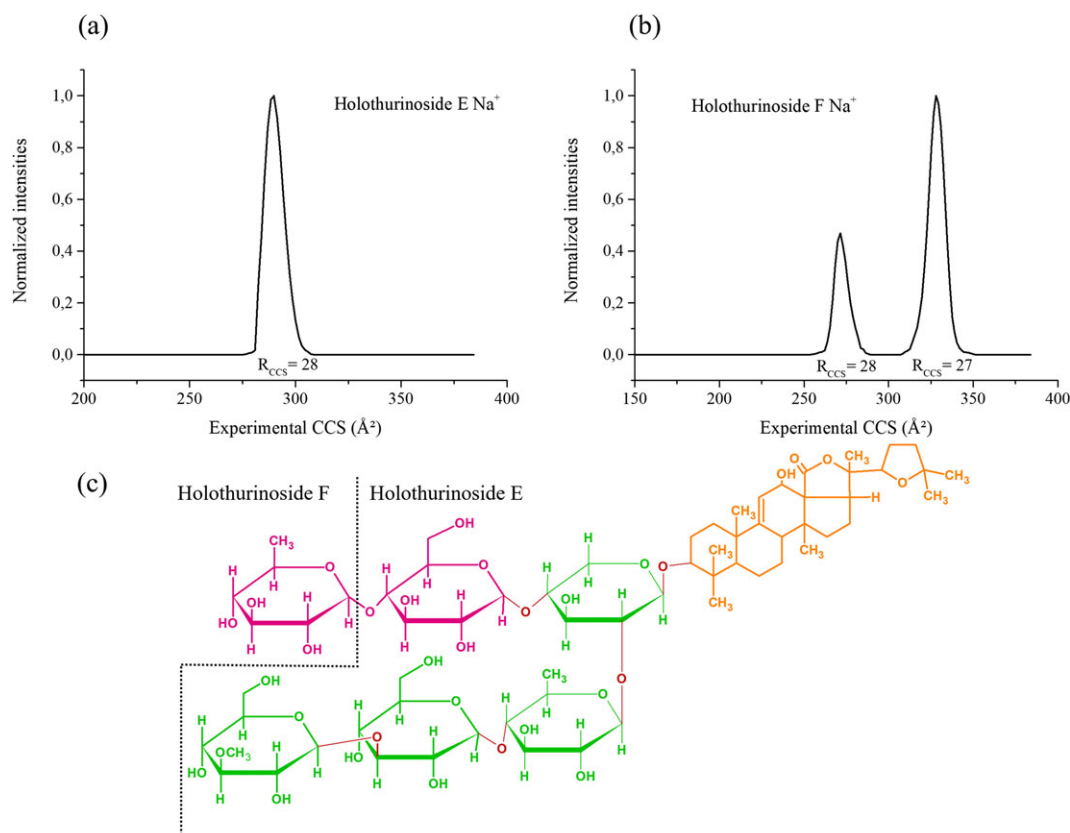


FIGURE 2 Ion mobility mass spectrometry analysis of saponin ions: (a) CCS distribution of the Na^+ adduct of Holothurinoside E; (b) CCS distribution of the Na^+ adduct of Holothurinoside F and (c) molecular structures of Holothurinosides E and F. The CCS resolutions (R_{CCS}) are determined for each ATD (see section 2.2) [Color figure can be viewed at wileyonlinelibrary.com]

cations are likely to interact differently with the saponin molecules. When analyzing the CCS_{exp} values in Figure 1, several aspects are worth stressing. First, the di- to pentasaccharide saponin ions are associated with single *Arrival Time Distributions* (ATD), whereas, for the hexasaccharide saponins, two different ion populations are clearly resolved for the $[M + Na]^+$ and $[M + K]^+$ ions, but not for the protonated saponins (see Figure 2 for typical examples). The presence of several peaks in the ATD for one species is often related to the coexistence of different conformational families with distinct CCS .⁵⁶ Spectral features broader than the expected peak width, which can be estimated based on the instrument resolution ($R_{CCS} = 40$ for the Waters Synapt G2-Si⁵⁷), may also be interpreted as originating from different structures. We measured ion mobility resolutions (R_{CCS}) around 30 for all observed ion mobility signals (see section 2) indicating the presence of unique rigid ion structures or fast interconverting ion structures.⁵⁶

The $[M + H]^+$ and $[M + Na]^+$ ions are most often associated with larger CCS_{exp} values than their K^+ counterparts, implying that cationization by K^+ induces a better compaction than H^+ and Na^+ additions. This is readily associated with the larger ionic radius of the K^+ ion (1.38 Å vs 1.02 Å for Na^+) inducing a better complexation of the cation – exploiting distant oxygen atoms on the molecular structure – and consequently affording more compact structures.

The $\langle CCS_{exp} \rangle$ globally increases with increasing number of monosaccharide residues, except for the tetra- and hexasaccharide saponins (except for the K^+ adducts) that are more compact than the tri- and pentasaccharide saponin ions, respectively. The observed reduction in $\langle CCS_{exp} \rangle$ from the 3- to 4-sugar saponin ions – despite the extra sugar – indicates that the lactone ring (Schemes 1a and 1b) of the sea cucumber sapogenin (4-sugar saponins) must participate in the charge stabilization, whatever the cation, and consequently forces the saccharide chain to lie over the aglycone part. On the other hand, we believe that the additional sugar when passing from the 5- to the 6-sugar saponins (identical sapogenin) is now involved in the charge stabilization, compacting therefore the ion structure for the smallest H^+ and Na^+ ions, as presented in Figure 1. For the $[M + K]^+$ saponin ions, the extra sugar (going from 5- to 6-sugar) does not on average impact the CCS values, probably because the $[M + K]^+$ 5-sugar saponin ions are already nicely folded due to the size of the K^+ cation.

When considering the evolution of the CCS_{exp} of saponin ions for a given number of saccharide residues, we observe that the differences in measured CCS_{exp} values are rather weak, except for Soyasaponins β_a and β_g , that appear less compact than the other trisaccharide saponins whatever the cationization. This increase in CCS , when compared with the other soyasaponins, is associated with the presence of the DDMP (2,3-Dihydro-2,5-Dihydroxy-6-Methyl-4-Pyrone) group (see Figure S1, supporting information) at the C23 position. Holothurinosides A and N also present significantly more extended ion structures than the other pentasaccharide saponins but only when potassium adducts are considered. The additional OH group (at the R_2 position in Scheme 1) on the sapogenins of Holothurinosides A and N when compared with Holothurinoside E (see Figure S3, supporting information) – and probably the unknown molecule – must participate in the K^+ ion stabilization. These experimentally driven conclusions will be compared with the candidate structures obtained upon MD simulations (see section 2) in the following section.

Nevertheless, before running MD simulations, we must first explicitly define the protonation site of the saponin molecules; in contrast, MD simulations are able to sample several positions of the Na^+ and K^+ cations in the $[M + Na]^+$ and $[M + K]^+$ ions (see section 2). For the protonated molecules, the C=C double bond present within the aglycone part (sapogenol/oleanic acid – see Scheme 1a) of soy and quinoa saponins is likely to be the most basic site since the protonation will afford a stabilized ternary carbocation. However, for the sea cucumber saponins (Scheme 1b), two different protonation sites must be considered, the C=C double bond and the lactone function. DFT calculations demonstrate that the lactone function possesses a slightly higher proton affinity than the C=C bond ($PA_{Lactone} = 938$ kJ/mol > $PA_{Double\ bond} = 935$ kJ/mol).⁵⁸ Therefore, we will consider in the MD simulations C-protonation and O-protonation for the soya/quinoa saponins and sea cucumber molecules, respectively.

Figure 3 schematically represents the optimized structures of all saponin ions to help to visualize their 3D structures. Disaccharide saponin ions – $[M + H]^+$, $[M + Na]^+$ and $[M + K]^+$ – are characterized by similar CCS values, around 230 Å². The most stable structures generated by MD simulations are presented in the case of Soyasaponin III as a representative example (see Figure 3). The detailed molecular structures are presented in Figure S5 (supporting information). The comparison between CCS_{th} and CCS_{exp} confirms that the MD-generated structures represent good candidates for the saponin ions (Figure 3). For the $[M + Na]^+$ and $[M + K]^+$ saponin ions, the cation is mostly localized on the disaccharide moiety though the oxygen atom of the hydroxyl group at the C24 position of the aglycone is also involved in the stabilization of the alkaline cation (see Scheme 1 and Figure S5, supporting information). For the protonated molecule, the proton is attached on the aglycone part at the C12 position and consequently remains too far from the short saccharide chain to enter into any interaction with the oxygen atoms. For the trisaccharide soyasaponins, the $[M + K]^+$ ions are the most compact saponin ions with a reduction in CCS of about 20 Å² when compared with the $[M + H]^+$ and $[M + Na]^+$ ions. As schematized in Figure 3 and detailed in Figure S5 (supporting information), for the $[M + Na]^+$ and $[M + K]^+$ ions, the alkaline cations are interacting with saccharide oxygen atoms. However, whereas the K^+ ion is interacting with the oxygen atoms of the first and second saccharide residues, the Na^+ interactions involve the first and the third residues (see Figure S5, supporting information). This difference in interactions, associated with the difference in size between the cations, allows the aglycone part to come closer (inducing a reduction in CCS) to the saccharide chains for the K^+ cationization. For the protonated molecules (aglycone C-protonation), the third monosaccharide residue that is added when going, for instance, from the Soyasaponin III (disaccharide) to Soyasaponin I (trisaccharide) is not interacting with the charged site, preserving the less compact ion structures generated upon protonation.

As previously mentioned, the tetrasaccharide (*Holothurinoside*) saponin ions appear more compact, whatever the cationization agent, than the trisaccharide derivatives (*Soyasaponin*). When comparing the aglycones of both families of saponins (Schemes 1a and 1b), we already anticipated that this is probably due to the presence of the lactone function on the holothurinoside sapogenins. This is definitively the case for the protonated saponins since the proton is localized on the oxygen atom of the lactone ring. Figure S5 (supporting

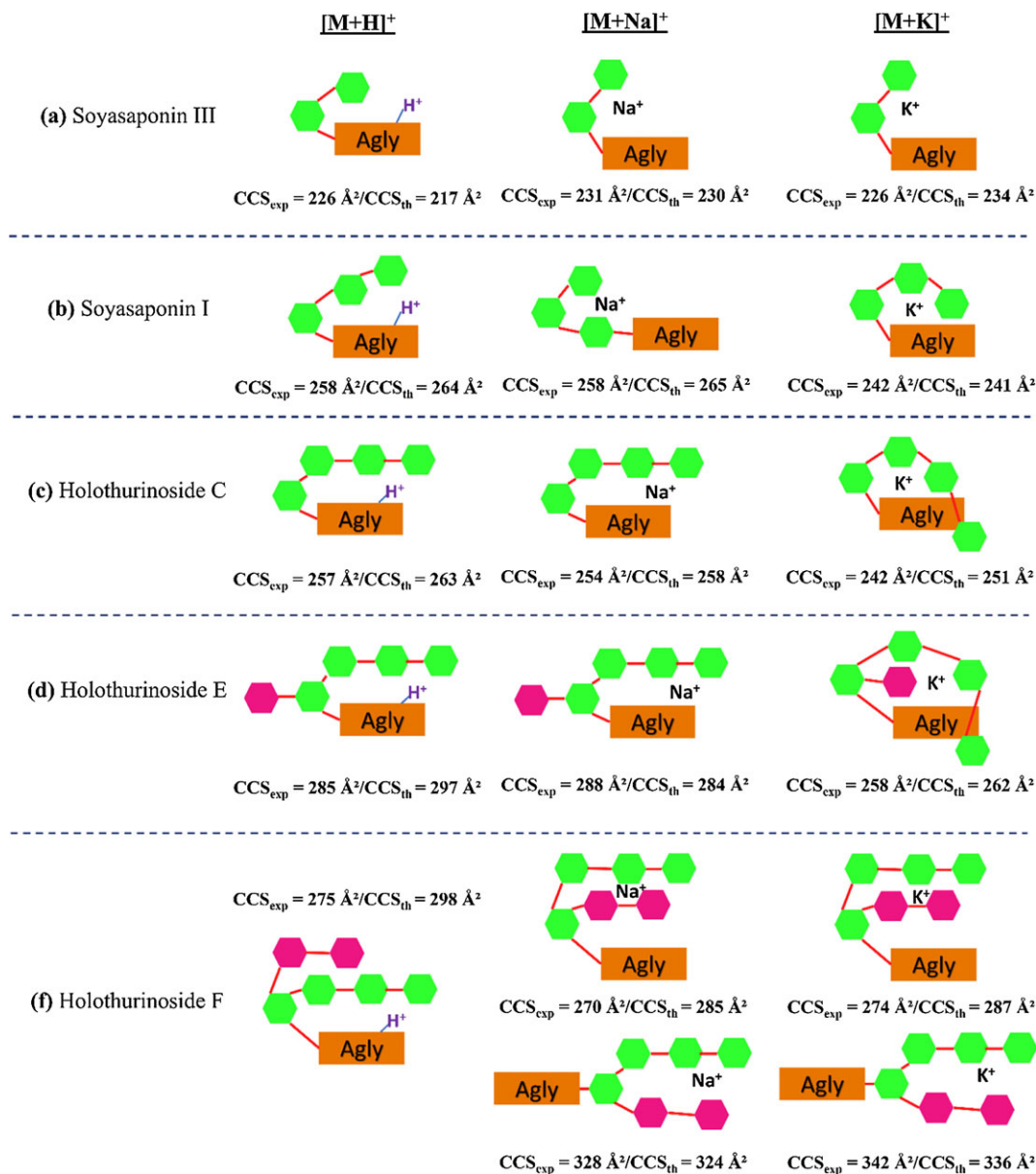


FIGURE 3 Schematic representations of the lowest energy ion structures obtained by Molecular Dynamics for the $[M + H]^+$, $[M + Na]^+$ and $[M + K]^+$ ions for monodesmosidic saponins presenting from 2 to 6 monosaccharides [Color figure can be viewed at wileyonlinelibrary.com]

information) presents the MD-generated structures for the $[M + H]^+$, $[M + Na]^+$, and $[M + K]^+$ ions of Holothurinoside C and they are schematized in Figure 3. As suggested by the similarity in their CCS_{exp} values (257 and 254 \AA^2), the $[M + H]^+$ and $[M + Na]^+$ ions possess similar V-shape structures triggered by the charge stabilization (Na^+ and H^+) by oxygen atoms present at the non-reducing end of the glycone section and the lactone oxygen atoms of the aglycone part. When analyzing the $[M + K]^+$ ion structure, we observe that the larger K^+ ions are interacting with oxygen atoms of both the aglycone and glycone moieties, though the involved oligosaccharide oxygen atoms only belong to the second monosaccharide residue. As a result, a slightly more folded structure is obtained when compared with the $[M + H]^+$ and $[M + Na]^+$ ions. The presence of the lactone function on the aglycone is thus at the origin of the more pronounced folding of the tetrasaccharide sea cucumber saponin ions when compared with the trisaccharide soy saponin ions.

Regarding the pentasaccharide saponin ions, we must first recall that the additional monosaccharide creates a ramification in the oligosaccharide chain, as presented in Figures 1 and S3 (supporting information). For the $[M + H]^+$ and $[M + Na]^+$ ions, the presence of this fifth residue has a significant impact on the saponin ion structure with a significant increase in the CCS when compared with the 4-sugar congeners, allowing the conclusion that this additional sugar does not participate in the charge stabilization. The gas-phase structures of the $[M + H]^+$ and $[M + Na]^+$ ions must be similar since their CCSs are close to one another. This is no longer the case for the $[M + K]^+$ ions that experience a global folding of the structure around the K^+ ion, affording a more compact structure. Based on MD calculations on Holothurinoside E as a typical example, we observed that indeed the additional residue does not interact with the charged site of the saponin ions for the $[M + H]^+$ and $[M + Na]^+$ ions, but interacts with the larger K^+

ion within the $[M + K]^+$ ions, see Figure S6 (supporting information) for the detailed molecular structures and Figure 3 for schematic interactions.

Finally, for the hexasaccharide congeners, the $[M + H]^+$ ions of Holothurinose F are characterized by a single ATD (Figure 1). When comparing again the 5- and 6-sugar saponins, it is interesting to note that the additional monosaccharide is associated with a more compact gas-phase structure. By analyzing the MD structures in Figure S6 (supporting information) and Figure 3, we realize that the additional sugar residue is not directly interacting with the protonated site but is lying close to the longest arm of the oligosaccharide chain, creating a compact gas-phase structure. As presented in Figures 1 and 2, the $[M + Na]^+$ and $[M + K]^+$ ions present however two ATDs, corresponding to two resolved ion structures. The compact structures present CCS_{exp} values around 275 \AA^2 (270 and 274 \AA^2 for the Na^+ and K^+ adducts, respectively), whereas the extended structures are characterized by CCS_{exp} values of 328 (Na^+) and 342 (K^+) \AA^2 . The folded structures of the $[M + Na]^+$ and $[M + K]^+$ ions are calculated to be really similar, in agreement with their similar CCS_{exp} values (Figure S6, supporting information), with the alkaline cation located between the two parts of the branched oligosaccharide chains, as represented in Figure 3. Interestingly, the MD data point to the fact that the lactone oxygen atoms are no longer interacting with the cation (Na^+ and K^+) for the hexasaccharidic saponins. Whereas K^+ complexation was previously shown to induce the folding of the saponins around the larger cation, it is worth pointing out that the replacement of the Na^+ cation by a K^+ cation induces a slight increase in CCS for the hexasaccharidic saponin ions, from 270 to 274 \AA^2 (see Figure 3). This structural expansion is even more pronounced when examining the extended saponin ions, passing from $CCS_{exp} = 328$ to 342 \AA^2 . The extended $[M + Na]^+$ and $[M + K]^+$ ions present similar structures with the Na^+/K^+ ion located between the two branches of the oligosaccharide part, whereas the lactone oxygen atoms of the aglycone moiety remain excluded from the global structure.

3.3 | Bidesmosidic topology analysis

The bidesmosidic saponins are extracted from *Glycine max* (soy) and *Chenopodium quinoa* and possess two different aglycones, as presented in Scheme 1. When exposed to IMMS measurements, all bidesmosidic saponin ions are associated with single *Arrival Time Distributions* (ATDs). The CCS_{exp} values of the different ionized bidesmosidic saponins, $[M + H]^+$, $[M + Na]^+$ and $[M + K]^+$, are measured and compared in Figure 4. The CC_{exp} values are grouped per increasing number of monosaccharide residues, i.e., trisaccharides with the (2 + 1) connectivity, (3 + 1) and (2 + 2) tetrasaccharides, and (3 + 2) pentasaccharides. Again, special attention is paid to the influence of different cationizing agents, i.e., H^+ , Na^+ and K^+ . We already described in the previous section that the C=C bond is most likely involved in the protonation of both families of saponins whereas the Na^+ and K^+ ions are free to move all along the saponin backbone to afford the most stable ion structure.

When analyzing the CCS_{exp} evolution, several aspects have to be stressed. First, contrary to what is observed for the monodesmosidic molecules, the $[M + Na]^+$ and $[M + K]^+$ ions are likely to adopt similar 3D structures with nearly identical CCS_{exp} values. Secondly, the $[M + H]^+$ ions always correspond to the most extended gas-phase structures with the highest CCS_{exp} ; this is especially conspicuous for the Soyasaponins A4 and A5. There is also a significant increase in CCS when passing from the tri- to the tetrasaccharides for all $[M + H]^+$, $[M + Na]^+$ and $[M + K]^+$ ions. However, when comparing the CCS_{exp} values of the tetra- and pentasaccharides, the increase in CCS is only remarkable for the $[M + H]^+$ ions. In Figure 5, we compare the MD-generated structures for the $[M + H]^+$ and $[M + Na]^+$ ions of Soyasaponin A4 which is a (3 + 2) bidesmosidic pentasaccharide saponin. The theoretical data nicely reproduce the CCS_{exp} . When analyzing the $[M + Na]^+$ structure, we realize that the Na^+ ion is in close interaction with the oxygen atoms of the trisaccharide branch. In addition, the disaccharide chain bends itself over the trisaccharide arm to create a compact structure, characterized

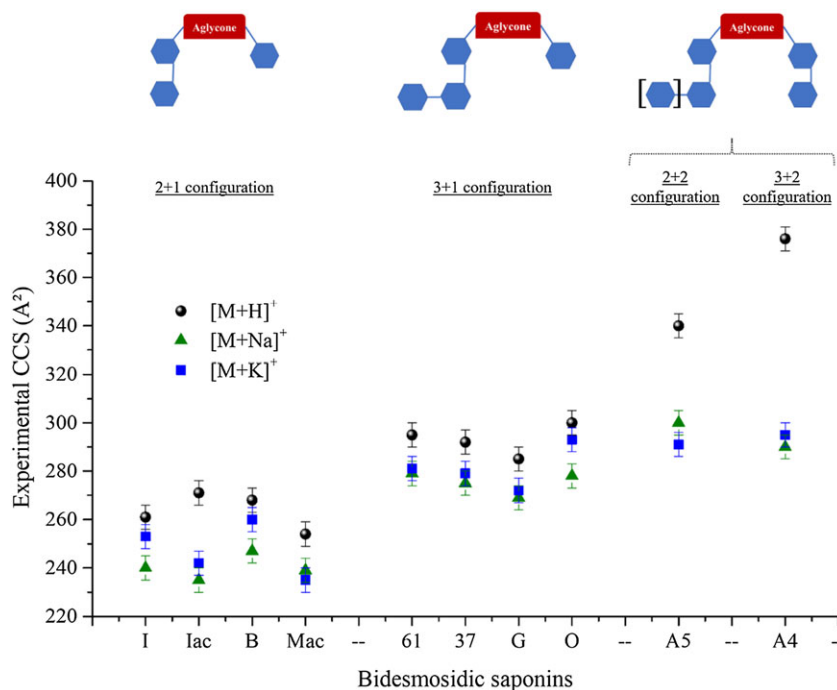


FIGURE 4 Experimental CCS for bidesmosidic saponin ions: comparison between the $[M + H]^+$ (black), $[M + Na]^+$ (green) and $[M + K]^+$ (blue) ions. The x-axis corresponds to the different saponins investigated in the present work and labelled according to their name, see Table 1 for the correspondence. Standard deviation <2%. The black circles, green triangles and blue squares respectively correspond to the $[M + H]^+$, $[M + Na]^+$ and $[M + K]^+$ ions for each saponin [Color figure can be viewed at wileyonlinelibrary.com]

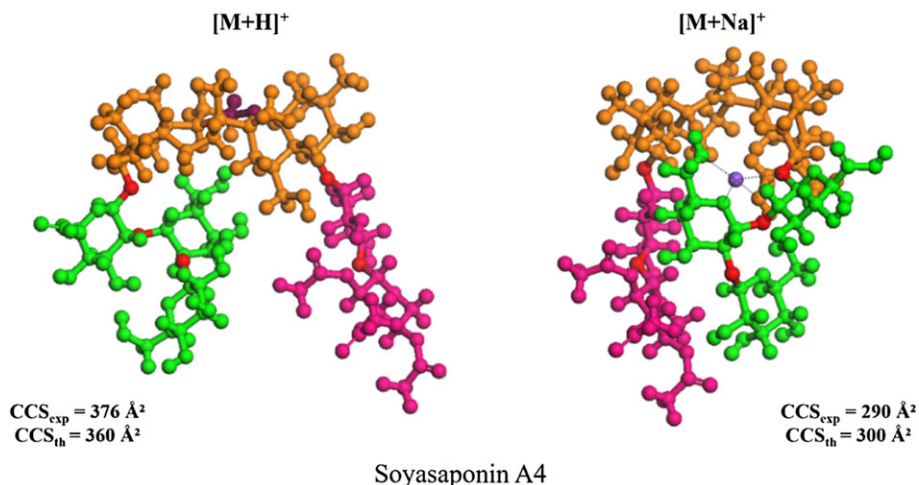


FIGURE 5 Optimized ion structures of the $[M + H]^+$ and $[M + Na]^+$ ions of Soyasaponin A4. The aglycone part is colored in orange. The glycone is colored in green and pink, respectively, for the oligosaccharides attached in C3 or C22 on the aglycone, and the glycoside bonds are in red. The electrostatic interactions are indicated with black dotted lines to show interactions between the cation, in purple, and oxygen atoms [Color figure can be viewed at wileyonlinelibrary.com]

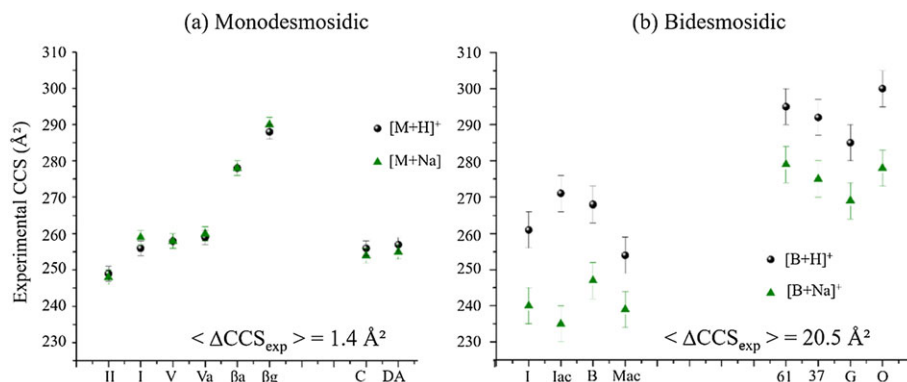


FIGURE 6 Comparison between the experimental CCSs measured for the $[M + H]^+$ and $[M + Na]^+$ ions of (a) monodesmosidic and (b) bidesmosidic saponins with 3 and 4 monosaccharide residues. The black circles and green triangles respectively correspond (a) to the $[M + H]^+$ and $[M + Na]^+$ ions for the monodesmosidic (M) saponins and (b) to the $[B + H]^+$ and $[B + Na]^+$ ions for the bidesmosidic (B) saponins. The $\langle \text{CCS}_{\text{exp}} \rangle$ values are calculated by averaging $\Delta \text{CCS}_{\text{exp}} = \text{CCS}_{\text{exp}} [M + H]^+ - \text{CCS}_{\text{exp}} [M + Na]^+$ over the monodesmosidic and bidesmosidic saponins [Color figure can be viewed at wileyonlinelibrary.com]

by a CCS_{th} value of 300 \AA^2 . On the other hand, in the case of protonated Soyasaponin A4, no interaction is predicted between the saccharide oxygen atoms and the proton, leading to an extended stable ion structure marked by a CCS_{th} value of 360 \AA^2 .

3.4 | Monodesmosidic versus bidesmosidic saponins

In Figure 6, we compare the CCS_{exp} values of the $[M + H]^+$ and $[M + Na]^+$ saponin ions with special attention paid to the distinction between monodesmosidic and bidesmosidic saponins. $[M + Na]^+$ and $[M + H]^+$ monodesmosidic ions are characterized by similar CCSs with an average ΔCCS of 1.4 \AA^2 . On the other hand, for the bidesmosidic ions, significantly more compact structures are observed for the $[M + Na]^+$ species for which the CCS values are measured to be about 20 \AA^2 lower (10% more compact) than their protonated counterparts. Therefore, based on this observation and in the range of the investigated molecules, if similar CCS values are measured for $[M + H]^+$ and $[M + Na]^+$ saponin ions, we can expect that we are facing a monodesmosidic topology.

This clearly represents an added value of IMMS when compared with CID mass spectrometry. Indeed, saponin ions mainly decompose upon CID by monosaccharide losses by competitive dissociation at the glycosidic bonds. In previous publications,³¹ we advantageously used tandem mass spectrometry to sequence the saccharide chain of saponin ions. CID spectra can also be helpful to distinguish isomeric saponins presenting branched and linear saccharide chains.³¹ However, branched and bidesmosidic saponin ions are hardly distinguished by CID since it is not straightforward to establish whether the monosaccharide residues are lost from two separated oligosaccharide chains (in bidesmosidic molecules) or from the two extremities of a branched oligosaccharide chain.

4 | CONCLUSIONS

In this present contribution, we applied ion mobility mass spectrometry together with computational chemistry for the structural characterization of saponins. Based on literature data, we sampled a

broad structural selection of saponin molecules in terms of the number of saccharide units and their topology, including monodesmosidic and bidesmosidic saponins. We submitted the $[M + H]^+$, $[M + Na]^+$ and $[M + K]^+$ saponin ions to IMMS in order to obtain experimental CCS values and to molecular dynamics simulations to generate candidate ion structures. We demonstrated that ion mobility contributes to the structural characterization of saponins, since different saponin ions can present significantly distinct collisional cross sections. Depending on the nature of the cation (in the positive ion mode), the differences in CCS can also be exacerbated, optimizing the gas-phase separation. When associated with MD simulations, the CCS data can be used to describe at a molecular level the interactions between the cations, i.e., H^+ , Na^+ and K^+ , and the saponin molecules. In this sense, our work contributes to decipher the influence of the saponin, of the polysaccharide chain length and of the nature/size/localization of the cation on the gas-phase structure of saponin ions. However, the structural diversity and complexity of the saponins can definitively not be unraveled by a single numerical value, here the CCS. In other words, the structural characterization of unknown saponins will be difficult to achieve based on ion mobility mass spectrometry alone. However, indirect evidences are likely to be produced by a careful comparison with ion mobility data obtained on identified saponin molecules.

Regarding the monodesmosidic and bidesmosidic saponin ions, we observed that $[M + H]^+$ and $[M + Na]^+$ saponin ions present different mobilities depending on whether the molecule is monodesmosidic or bidesmosidic. Indeed, for the same number of monosaccharides, the $[M + Na]^+$ bidesmosidic ions are always significantly more compact than their $[M + H]^+$ homologues (about 10% reduction in CCS), whereas for the monodesmosidic molecules, the CCSs are almost identical for the $[M + H]^+$ and $[M + Na]^+$ ions. This difference is proposed as a characterization criterion to distinguish monodesmosidic and bidesmosidic saponins.

ACKNOWLEDGEMENTS

The MS laboratory acknowledges the "Fonds de la Recherche Scientifique" (FRS-FNRS) for its contribution to the acquisition of the Waters QToF Premier and the Waters Synapt G2-Si mass spectrometers. Computational resources were provided by the Consortium des Équipements de Calcul Intensif (CÉCI) funded by F.R.S.-FNRS under Grant No. 2.5020.11. The work in the Laboratory for Chemistry of Novel Materials was supported by the European Commission/Région Wallonne (FEDER – BIORGEL project), the Interuniversity Attraction Pole program of the Belgian Federal Science Policy Office (PAI 7/05), and the Programme d'Excellence de la Région Wallonne (OPTI2MAT project). P.F. and J.C. are Research Directors of the FRS-FNRS. C.D. and E.C. are grateful to the F.R.I.A. for financial support. Part of the work (GCB) is supported by the project CONICYT PIA/APOYO CCTE AFB170007.

ORCID

Corentin Decroo  <http://orcid.org/0000-0001-7931-7120>

Vincent Lemaire  <http://orcid.org/0000-0001-8601-286X>

Guillaume Caulier  <http://orcid.org/0000-0001-7414-1226>

Julien De Winter  <http://orcid.org/0000-0003-3429-5911>

Jérôme Cornil  <http://orcid.org/0000-0002-5479-4227>

Patrick Flammang  <http://orcid.org/0000-0001-9938-1154>

Pascal Gerbaux  <http://orcid.org/0000-0001-5114-4352>

REFERENCES

- Maier MS. Biological activities of sulfated glycosides from echinoderms. *Stud Nat Prod Chem.* 2008;35:311-354.
- D'Aurla MV, Minale L, Riccio R. Polyoxygenated steroids of marine origin. *Chem Rev.* 1993;93:1839-1895.
- Zhao M, Ma NF, Qiu X, et al. Triterpenoid saponins from the roots of *Clematis argentea*. *Fitoterapia.* 2014;97:234-240.
- Zhang XF, Yang SL, Han YY, et al. Qualitative and quantitative analysis of triterpene saponins from tea seed pomace (*Camellia oleifera abel*) and their activities against bacteria and fungi. *Molecules.* 2014;19(6):7568-7580.
- Sparg SG, Light ME, Van Staden J. Biological activities and distribution of plant saponins. *J Ethnopharmacol.* 2004;94:219-243.
- Vanderplanck M, Declèves S, Roger N, et al. Is non-host pollen suitable for generalist bumblebees? *Insect Sci.* 2018;25(2):259-272.
- Iorizzi M, De Riccardis F, Minale L, Riccio R. Starfish saponins, 52. Chemical constituents from the starfish *Echinaster brasiliensis*. *J Nat Prod.* 1993;56(12):2149-2162.
- Palagiano E, Zollo F, Minale L, et al. Isolation of 20 glycosides from the starfish *Henricia downeyae*, collected in the Gulf of Mexico. *J Nat Prod.* 1996;59(4):348-354.
- Kicha AA, Kalinovsky AI, Malyarenko TV, et al. Cyclic steroid glycosides from the starfish *Echinaster luzonicus*: Structures and immunomodulatory activities. *J Nat Prod.* 2015;78(6):1397-1405.
- Ivanchina NV, Kicha AA, Malyarenko TV, et al. Biosynthesis of polar steroids from the Far Eastern starfish *Patiria (=Asterina) pectinifera*. Cholesterol and cholesterol sulfate are converted into polyhydroxylated sterols and monoglycoside asterosaponin P1 in feeding experiments. *Steroids.* 2013;78(12):1183-1191.
- Demeyer M, Wisztorzski M, Decroo C, et al. Inter- and intra-organ spatial distributions of sea star saponins by MALDI imaging. *Anal Bioanal Chem.* 2015;407:8813-8824.
- Caulier G, Mezali K, Soualili DL, et al. Chemical characterization of saponins contained in the body wall and the Cuvierian tubules of the sea cucumber *Holothuria (Platyperona) sanctori* (Delle Chiaje, 1823). *Biochem Syst Ecol.* 2016;68:119-127.
- Kalinin VI, Avilov SA, Silchenko AS, Stonik VA. Triterpene glycosides of sea cucumbers (Holothuroidea, Echinodermata) as taxonomic markers. *Nat Prod Commun.* 2015;10(1):21-26.
- Bahrami Y, Zhang W, Chataway T, Franco C. Structural elucidation of novel saponins in the sea cucumber *Holothuria lessona*. *Mar Drugs.* 2014;12(8):4439-4473.
- Honey-Escandon M, Arreguin-Espinosa R, Solis-Marin FA, Samyn Y. Biological and taxonomic perspective of triterpenoid glycosides of sea cucumbers of the family Holothuriidae (Echinodermata, Holothuroidea). *Comp Biochem Physiol Part B Biochem Mol Biol.* 2015;180:16-39.
- Van Dyck S, Gerbaux P, Flammang P. Elucidation of molecular diversity and body distribution of saponins in the sea cucumber *Holothuria forskali* (Echinodermata) by mass spectrometry. *Comp Biochem Physiol Part B Biochem Mol Biol.* 2009;152(2):124-134.
- Van Dyck S, Gerbaux P, Flammang P. Qualitative and quantitative saponin contents in five sea cucumbers from the Indian ocean. *Mar Drugs.* 2010;8(1):173-189.
- Cuong NX, Vien LT, Hong Hanh TT, et al. Cytotoxic triterpene saponins from *Cercodemas anceps*. *Bioorg Med Chem Lett.* 2015;25(16):3151-3156.
- Saikia S, Kolita B, Dutta PP, et al. Marine steroids as potential anticancer drug candidates: In silico investigation in search of inhibitors of Bcl-2 and CDK-4/Cyclin D1. *Steroids.* 2015;102:7-16.
- Tseng WR, Huang CY, Tsai YY, et al. New cytotoxic and anti-inflammatory steroids from the soft coral *Klyxum flaccidum*. *Bioorg Med Chem Lett.* 2016;26(14):3253-3257.
- Mohanan P, Subramaniyam S, Mathiyalagan R, Yang DC. Molecular signaling of ginsenosides Rb1, Rg1, and Rg3 and their mode of actions. *J Ginseng Res.* 2016;9:1-10.

22. Petit PR, Sauvaire YD, Hillaire-Buys DM, et al. Steroid saponins from fenugreek seeds: Extraction, purification, and pharmacological investigation on feeding behavior and plasma cholesterol. *Steroids*. 1995;60(10):674-680.
23. Aminin DL, Chaykina EL, Agafonova IG, et al. Antitumor activity of the immunomodulatory lead Cumaside. *Int Immunopharmacol*. 2010;10(6):648-654.
24. Yoshikawa N, Harada M, Murakami E, et al. Escins-ia ib, iia, iib, and iiii, bioactive triterpene oligoglycosides from the seeds of *Aesculus hippocastanum* L.: Their inhibitory effects on ethanol absorption and hypoglycemic activity on glucose tolerance test. *Chem Pharm Bull(Tokyo)*. 1994;42(6):1357-1359.
25. Rodriguez J, Castro R, ChemInform Abstract RR. Holothurinosides: New antitumor non-sulfated triterpenoid glycosides from the sea cucumber *Holothuria forskalii*. *ChemInform*. 2010;22(36):4753-4763.
26. Minale L, Pizza C, Riccio R, Zollo F. Steroidal glycosides from starfishes. *Pure Appl Chem*. 1982;54(10):1935-1950.
27. Dang NH, Van Thanh N, Van Kiem P, et al. Two new triterpene glycosides from the Vietnamese sea cucumber *Holothuria scabra*. *Arch Pharm Res*. 2007;30(11):1387-1391.
28. Han H, Yi Y-H, Li L, et al. Triterpene glycosides from sea cucumber *Holothuria leucospilota*. *Chin J Nat Med*. 2009;7(5):346-350.
29. Berhow MA, Cantrell CL, Duval SM, et al. Analysis and quantitative determination of group B saponins in processed soybean products. *Phytochem Anal*. 2002;13(6):343-348.
30. Bahrami Y, Franco CMM, Mayer AM. Structure elucidation of new acetylated saponins, Lessoniosides A, B, C, D, and E, and non-acetylated saponins, Lessoniosides F and G, from the viscera of the sea cucumber *Holothuria lessona*. *Mar Drugs*. 2015;13:597-617.
31. Decroo C, Colson E, Demeyer M, et al. Tackling saponin diversity in marine animals by mass spectrometry: data acquisition and integration. *Anal Bioanal Chem*. 2017;409(12):3115-3126.
32. Xu W, Wu JM, Zhu Z, et al. Pentacyclic triterpenoid saponins from *Silene viscidula*. *Helv Chim Acta*. 2010;93(10):2007-2014.
33. Madl T, Sterk H, Mittelbach M, Rechberger GN. Tandem mass spectrometric analysis of a complex triterpene saponin mixture of *Chenopodium quinoa*. *J Am Soc Mass Spectrom*. 2006;17(6):795-806.
34. Kimura H, Ogawa S, Jisaka M, et al. Identification of novel saponins from edible seeds of Japanese horse chestnut (*Aesculus turbinata* Blume) after treatment with wooden ashes and their nutraceutical activity. *J Pharm Biomed Anal*. 2006;41(5):1657-1665.
35. Shi L, Holliday AE, Glover MS, et al. Ion mobility-mass spectrometry reveals the energetics of intermediates that guide polyproline folding. *J Am Soc Mass Spectrom*. 2016;27(1):22-30.
36. Duez Q, Josse T, Lemaury V, et al. Correlation between the shape of the ion mobility signals and the stepwise folding process of polylactide ions. *J Mass Spectrom*. 2017;52(3):133-138.
37. Both P, Green AP, Gray CJ, et al. Discrimination of epimeric glycans and glycopeptides using IM-MS and its potential for carbohydrate sequencing. *Nat Chem*. 2014;6(1):65-74.
38. Li H, Giles K, Bendiak B, et al. Resolving structural isomers of monosaccharide methyl glycosides using drift tube and traveling wave ion mobility mass spectrometry. *Anal Chem*. 2012;84(7):3231-3239.
39. Reddy AV, Ravinder K, Narasimhulu M, et al. New anticancer bastadin alkaloids from the sponge *Dendrilla cactos*. *Bioorg Med Chem*. 2006;14(13):4452-4457.
40. Chalet C, Hollebrands B, Janssen H-G, Augustijns P, Duchateau G. Identification of phase-II metabolites of flavonoids by liquid chromatography-ion-mobility spectrometry-mass spectrometry. *Anal Bioanal Chem*. 2017;409:1-12.
41. Gonzales GB, Raes K, Coelus S, et al. Ultra (high)-pressure liquid chromatography-electrospray ionization-time-of-flight-ion mobility-high definition mass spectrometry for the rapid identification and structural characterization of flavonoid glycosides from cauliflower waste. *J Chromatogr A*. 2014;1323:39-48.
42. Yassin GH, Grun G, Koek JH, Assafa KI, Kuhnert N. Investigation of isomeric flavanol structures in black tea thearubigins using ultraperformance liquid chromatography coupled to hybrid quadrupole/ion mobility/time of flight mass spectrometry. *J Mass Spectrom*. 2014;49:1086-1095.
43. Bataglion GA, Martins H, Souza F, et al. Separation of glycosidic cationomers by TWIM-MS using CO₂ as a drift gas. *J Mass Spectrom*. 2015;50:336-343.
44. Elias R, Diaz Lanza AM, Vidal-Ollivier E, Balansard G. Triterpenoid saponins from the leaves of *Hedera helix*. *J Nat Prod*. 1991;54(1):98-103.
45. Tchoukoua A, Tabopda TK, Uesugi S, et al. Triterpene saponins from the roots of *Acacia albida* Del. (Mimosaceae). *Phytochemistry*. 2017;136:31-38.
46. Acebey-Castellon IL, Voutquenne-Nazabadioko L, Doan Thi Mai H, et al. Triterpenoid saponins from *Symplocos lancifolia*. *J Nat Prod*. 2011;74(2):163-168.
47. Kudou S, Tonomura M, Tsukamoto C, et al. Isolation and structural elucidation of DDMP-conjugated soyasaponins as genuine saponins from soybean seeds. *Biosci Biotechnol Biochem*. 1993;57(4):546-550.
48. Zhang W, Popovich DG. Chemical and biological characterization of oleanane triterpenoids from soy. *Molecules*. 2009;14(8):2959-2975.
49. Dini I, Tenore GC, Dini A. Oleanane saponins in "kancolla", a sweet variety of *Chenopodium quinoa*. *J Nat Prod*. 2002;65(7):1023-1026.
50. Duez Q, Chirot F, Liénard R, et al. Polymers for traveling wave ion mobility spectrometry calibration. *J Am Soc Mass Spectrom*. 2017;28(11):2483-2491.
51. Mayo SL, Olafson BD, Goddard WA III. DREIDING: A generic force field for molecular simulations. *J Phys Chem*. 1990;101(540):8897-8909.
52. Accelrys Software Inc. MS Modeling. 2011.
53. Rappé AKK, Casewit CJJ, Colwell KSS, et al. UFF, a full Periodic Table force field for molecular mechanics and molecular dynamics simulations. *J Am Chem Soc*. 1992;114(25):10024-10035.
54. Mesleh MF. Structural information from ion mobility measurements: Effects of the long-range potential. *J Phys Chem*. 1996;100:16082-16086.
55. Shvartsburg AA, Jarrold MF. An exact hard-spheres scattering model for the mobilities of polyatomic ions. *Chem Phys Lett*. 1996;261:86-91.
56. Giles K, Williams JP, Campuzano I. Enhancements in travelling wave ion mobility resolution. *Rapid Commun Mass Spectrom*. 2011;25:1559-1566.
57. Poyer S, Comby-Zerbino C, Choi CM, et al. Conformational dynamics in ion mobility data. *Anal Chem*. 2017;89:4230-4237.
58. These PA values are validated by comparison with the PA values of two reference molecules, 1-methylcyclohexene and butyrolactone, that amount to 825 and 840 kJ/mol, respectively. Hunter EP, Lias SG. Evaluated gas phase basicities and proton affinities of molecules: an update. *J Phys Chem Ref Data Monogr*. 1998;27:413-656.

SUPPORTING INFORMATION

Additional supporting information may be found online in the Supporting Information section at the end of the article.

How to cite this article: Decroo C, Colson E, Lemaury V, et al. Ion mobility mass spectrometry of saponin ions. *Rapid Commun Mass Spectrom*. 2018;1-12. <https://doi.org/10.1002/rcm.8193>